# *An automatic and quantitative approach to the detection and tracking of acoustic scattering layers*





| | |
|---|---|
| **Citation** | Cade, D. E., & Benoit-Bird, K. J. (2014). An automatic and quantitative approach to the detection and tracking of acoustic scattering layers. Limnology and Oceanography: Methods, 12, 742-756. doi:10.4319/lom.2014.12.742 |
| **DOI** | 10.4319/lom.2014.12.742 |
| **Publisher** | American Society of Limnology and Oceanography, Inc. |
| **Version** | Version of Record |
| **Terms of Use** | http://cdss.library.oregonstate.edu/sa-termsofuse |

LIMNOLOGY
and
OCEANOGRAPHY: METHODS

*Limnol. Oceanogr.: Methods* 12, 2014, 742–756


# An automatic and quantitative approach to the detection and tracking of acoustic scattering layers

*David E. Cade*[1] *and Kelly J. Benoit-Bird*[1*]

[1]College of Earth, Ocean and Atmospheric Sciences (CEOAS), Oregon State University, 104 CEOAS Administration Bldg., Corvallis, OR 97331, USA

## *Abstract*

Acoustic scattering layers are ubiquitous, horizontally extensive aggregations of both vertebrate and invertebrate organisms that play key roles in oceanic ecosystems. However, currently there are no conventions or widely adaptable automatic methods for identifying these often dynamic, spatially complex features, so it is difficult to consistently and efficiently describe and compare results. We developed an automatic scattering layer detection method that can be used to monitor changes in layer depth, width, and internal structure over time. Extensive, contiguous regions of the water column that have echo strengths above a threshold were identified as "background layers." They correspond to regions of the water column that contain scattering from diffusely distributed organisms. Often, background layers contained contiguous, horizontally extensive features of concentrated acoustic scattering we identified as "strata." These features were identified by fitting Gaussian curves to the echo envelope of each vertical profile of scattering, and their boundaries were identified as the endpoints of the region containing 95% of the area under the fitted curves. These endpoints were linked horizontally to make continuous tracks. Bottom and top tracks were paired to identify features that sometimes extended horizontally for tens of kilometers. This approach was effective in three disparate ecosystems (the Gulf of California, Monterey Bay, and the Bering Sea), and a sensitivity analysis showed its robustness to changes in input parameters. By allowing a comparable, automated approach to be used across environments, this method promotes the improved classification and characterization of acoustic scattering layers necessary for examining their role in oceanic ecosystems.

Since the first explorations of the ocean with sonar in the 1940s, oceanographers have consistently identified intense mid-water sound scattering layers (Duvall and Christensen 1946) that appear in echograms as continuous features in which individual organisms cannot be resolved (Tont 1976). Scattering layers are found in all oceans (O'Brien 1987; Tont 1976) and are the result of acoustic scattering from extensive aggregations of micronekton and large zooplankton. Physically, scattering layers can extend for hundreds of kilometers horizontally (Chapman and Marshall 1966), be on the order of meters to tens of meters thick (Sameoto 1976; Thomson et al. 1992), and can be found from near the surface to depths greater than 2000 m (Burd et al. 1992; Opdal et al. 2008). The organisms that make up these layers are important parts of the diets of creatures ranging from squid to fish to birds to mammals (Hays 2003; Markaida et al. 2008) and thus are vital links between primary productivity and the higher trophic levels of marine ecosystems. Many species contained in scattering layers undertake a diel vertical migration (DVM) from deep water to the surface that has been shown to make important contributions to the active cycling of carbon and nutrients (Steinberg et al. 2000).

Prior research into sound scattering layers has focused on their composition, their DVM, the forcing mechanisms of their migrations and their role in various ecosystems (e.g., Hays 2003; Tont 1976). However, despite this research into scattering layer behavior and biology, questions about scattering layer constituents, biomass, spatial dynamics, and ecological significance remain. Addressing these questions is made challenging because there are no standardized tools available

*Corresponding author: E-mail: kbenoit@coas.oregonstate.edu

***Acknowledgments***

The authors wish to thank Chad Waluk for technical assistance, Sarah Emerson for consultations on statistics, and Marisa Litz, Emily Shroyer, and Scott Heppell for helpful comments. We thank the US Office of Naval Research (N00014-11-1-0146) for dedicated support of the data analysis and the National Science Foundation (0851239), North Pacific Research Board (Bering Sea Projects B67 and B77), and the US Office of Naval Research (N0014-05-1-0608) for supporting the collection of the data used.

DOI 10.4319/lom.2014.12.742

for identifying layers or even agreed upon conventions for describing basic features of scattering layers (i.e., determining their boundaries, characterizing their acoustic structure, and describing their depth). While some authors measure the depth of a layer in the water column from the top boundary (Baliño and Aksnes 1993; Tont 1976), others focus on the bottom (Kumar et al. 2005), and others on the depth of peak energy (Benoit-Bird et al. 2010). However, layers can have variable internal structure and can be more than 100 m thick, so considering only one measure of depth within the water column may be insufficient for studying the response of scattering layers to oceanographic parameters. Additionally, describing acoustic structure within scattering layers has had only limited emphasis in the literature (e.g., Benoit-Bird and Au 2003) despite evidence that this structure can have important implications for the ecology of scattering layer organisms (Benoit-Bird and McManus 2012).

Our goal was to create a method for automatic layer detection that could assist in addressing these research gaps by consistently quantifying the spatial characteristics of scattering layers. A number of approaches have been tried previously but have met with mixed success. The most common approaches have involved basic visual examination of echograms (e.g., Kumar et al. 2005; Robinson and Gómez-Gutiérrez 1998; Simard and Mackas 1989). This approach is simple, can be done in real-time for determining appropriate net trawl depths, and can be used to effectively determine layer boundaries even in acoustically complex environments; however, as with any procedure done by trained observers, results can vary between individuals as well as for one individual observer over time (as discussed in Jech and Michaels 2006). Visual identification is also laborious and can prove intractable due to the substantial volume of data that can be generated by acoustic instruments on ships and other platforms.

Another common approach has been to classify layers based on the broad depth bin in which acoustic energy is contained (i.e., surface, mesopelagic, epipelagic, and bathypelagic). This approach allows researchers to ignore the structure of layers and to focus solely on the acoustic energy that is present at a given depth of interest. While useful for studies of DVM and for wide area biomass surveys (e.g., Kloser et al. 2009), this approach does not allow individual features to be tracked, nor does it exclude acoustic energy that is not part of a scattering layer.

Automatic layer detection approaches have the potential to overcome the drawbacks of manual layer identification and depth-based layer definitions. To do so effectively they must locate the top and bottom of several layers in the water column, identify layers with a variety of acoustic structures, be effective in a range of locations with differing biological layer compositions, respond predictably to changes in input parameters, and account for horizontally extensive layers that can change their depth in the water column and can split and merge over time. A typical automated approach looks for the sharpest gradient in the water column. Often used for seafloor detection, such approaches can be adept at locating the depth of long, continuous features. These types of algorithms, however, locate only a single depth and thus ignore layer thickness. It can also be difficult for seafloor detection methods to consistently locate biological layers since, unlike the seafloor that exhibits a sharp gradient in scattering relative to open water, scattering from biology typically diminishes from the peak more slowly and is only rarely characterized by a sudden increase or decrease in echo strength.

School detection algorithms (e.g., Barange 1994) have been adapted to identify scattering layers since they are designed to find the boundaries of discrete aggregations of organisms. Similar to many bottom detection algorithms, they work by looking for an amplitude difference between a region and its surrounding regions, typically searching for a value greater than a fixed threshold. As shown by Burgos and Horne (2007), however, the choice of acoustic threshold has a significant effect on the height, length, depth, and the total acoustic energy of the detected aggregations, so choosing an appropriate, robust acoustic threshold can be challenging. Weber et al. (2009) used a statistical approach to determine an appropriate noise-threshold for analysis of fish schools, relying on a controlled situation with data collected in the presence and absence of a single-species assemblage. Scattering layers, in contrast, pose a particularly challenging scenario since they are characterized by mixed species aggregations, are horizontally extensive, and often exist in regions with varying background conditions. Perhaps the most significant challenge for adapting school and patch detection algorithms to layers is the requirement that identified features be limited in their horizontal extent. Nero and Magnuson's (1992) patch detection algorithm, for example, limits the spatial extent of patches to the size of their chosen smoothing window, whereas Weill et al.'s algorithm (1993) must prematurely terminate long features. School detection algorithms also assume that features are relatively stable, yet scattering layers are defined partly by their evolution over time. Fig. 1, for example, features a deeper layer shoaling at sunset to meet a shallow layer. A school detection algorithm would treat these two features as a single combined aggregation despite clear differences in their behavior.

To account for properties unique to scattering layers, some novel approaches have been developed. Bertrand et al. (2010) successfully tracked the bottom of a layer of pelagic organisms by determining the depth at which 98% of accumulated echoes occurred. In their study area, this depth was shallow (<100 m) and characterized by a rapid build-up of echo energy at the base of the layer due to a strong oxycline. However, this approach is not effective for layers that have more graded changes in scattering or in regions containing several layers that distribute echo energy throughout the water column. Benoit-Bird and Au (2004) identified scattering layer boundaries based on differences in the numerical density of organ-

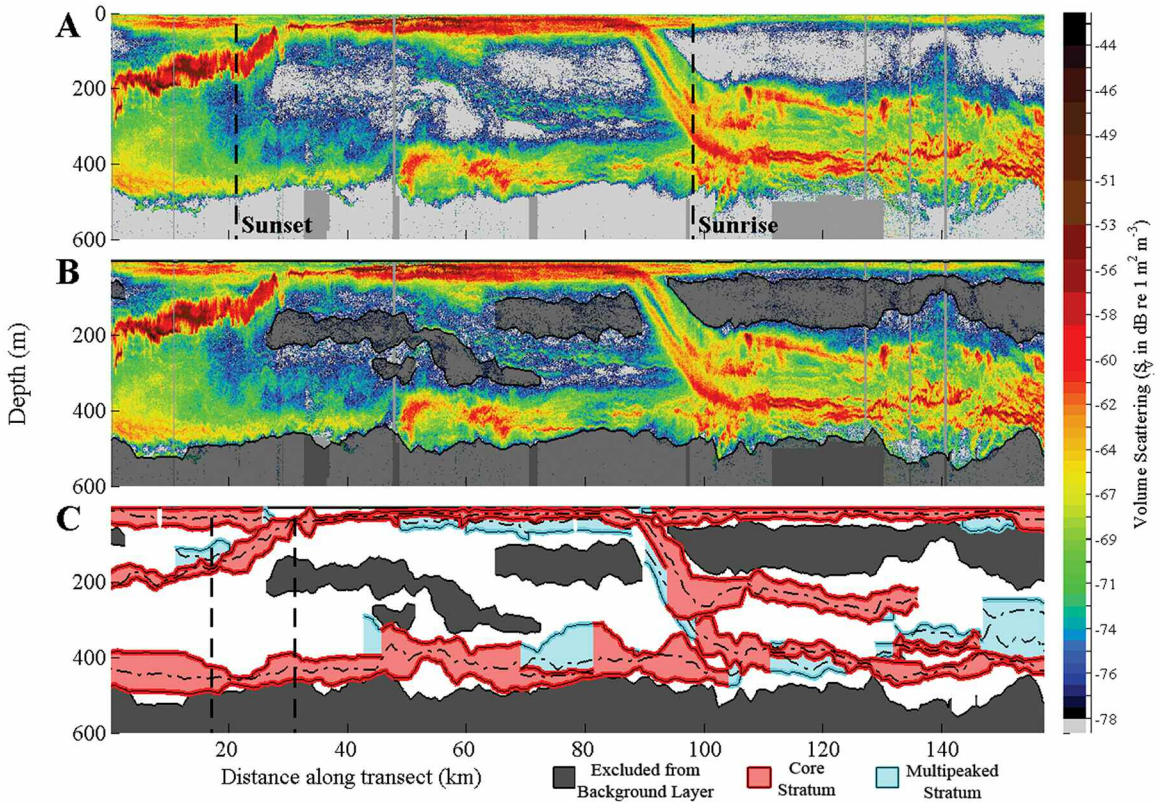


**Fig. 1.** A 150-km section of continuous 70 kHz echosoundings in the Gulf of California collected 9-10 Jun 2011. The Gulf of California is a sub-tropical sea with aggregations of euphausiids, squid, and myctophids (Benoit-Bird and Gilly 2012). (A) Data displayed have had the background noise removed and are averaged into 1 m vertical × 20 m horizontal bins. Diel vertical migration is apparent on either side of sunset and sunrise (indicated). (B) Background layers are outlined and regions of the water column not included in the background layers are darkened. Parameter values used for this detection are listed in Table 1. (C) Detected core strata (red) and multipeaked strata (blue) in the echogram from panel B. Regions not identified as belonging to a background layer are grayed out. The white regions are background layers that do not contain identified strata. The boundaries of the multipeaked strata encompass the adjoining core strata, and both types of strata are entirely contained within the background layers. The dashed lines are tracks of the horizontally contiguous peaks of the fitted Gaussians, and represent the depth of peak energy within each stratum. Vertical dashed lines at 17 and 31 km indicate the region displayed in Fig. 3.

isms in adjoining data windows, but this approach relies on detailed knowledge of the layer constituents and their acoustic properties to be applied. A more general approach is to use the characteristics of high-amplitude peaks in the echo intensity to determine layer boundaries (Benoit-Bird 2009; Cheriton et al. 2007), relying on a defined minimum peak amplitude above background levels, but again introducing the challenges of identifying an appropriate threshold value. Our goal was to further expand upon these layer-specific methods to develop and evaluate an approach to tracking and describing scattering layers that is applicable across ecosystems, allows for consistent descriptions of their depth, boundaries, and internal structure, and which can characterize the distribution of the echo strengths within each layer in a way that can be easily conceptualized.

## *Materials and procedures*

To provide comparative information about acoustic scattering layers, a detection algorithm must be able to monitor and describe acoustic scattering layers at a variety of depths, with varying internal acoustic structure, over extensive distances and in a variety of acoustic environments with varying data quality. To this end, we developed a layer detection and tracking algorithm, summarized in Fig. 2, using data collected in the subtropical Gulf of California (GoC) and employing Echoview version 5.2.7 (Myriax) and MATLAB version 8.1 (MathWorks). The online archive of the complete MATLAB code for this procedure, including the implementation and modifications of several preexisting subroutines, can be examined for additional specific details (Cade and Benoit-Bird 2014). The algorithm identified the boundaries of contiguous, horizontally extensive regions of scattering and characterized the internal structure of these features. We then tested our algorithm on data from two additional locations representing a range of physical and biological oceanographic conditions: the productive, temperate waters of Monterey Bay, California (MB) and the sub-arctic Bering Sea near the Pribilof Islands (PI). The resulting algorithm included ten different input

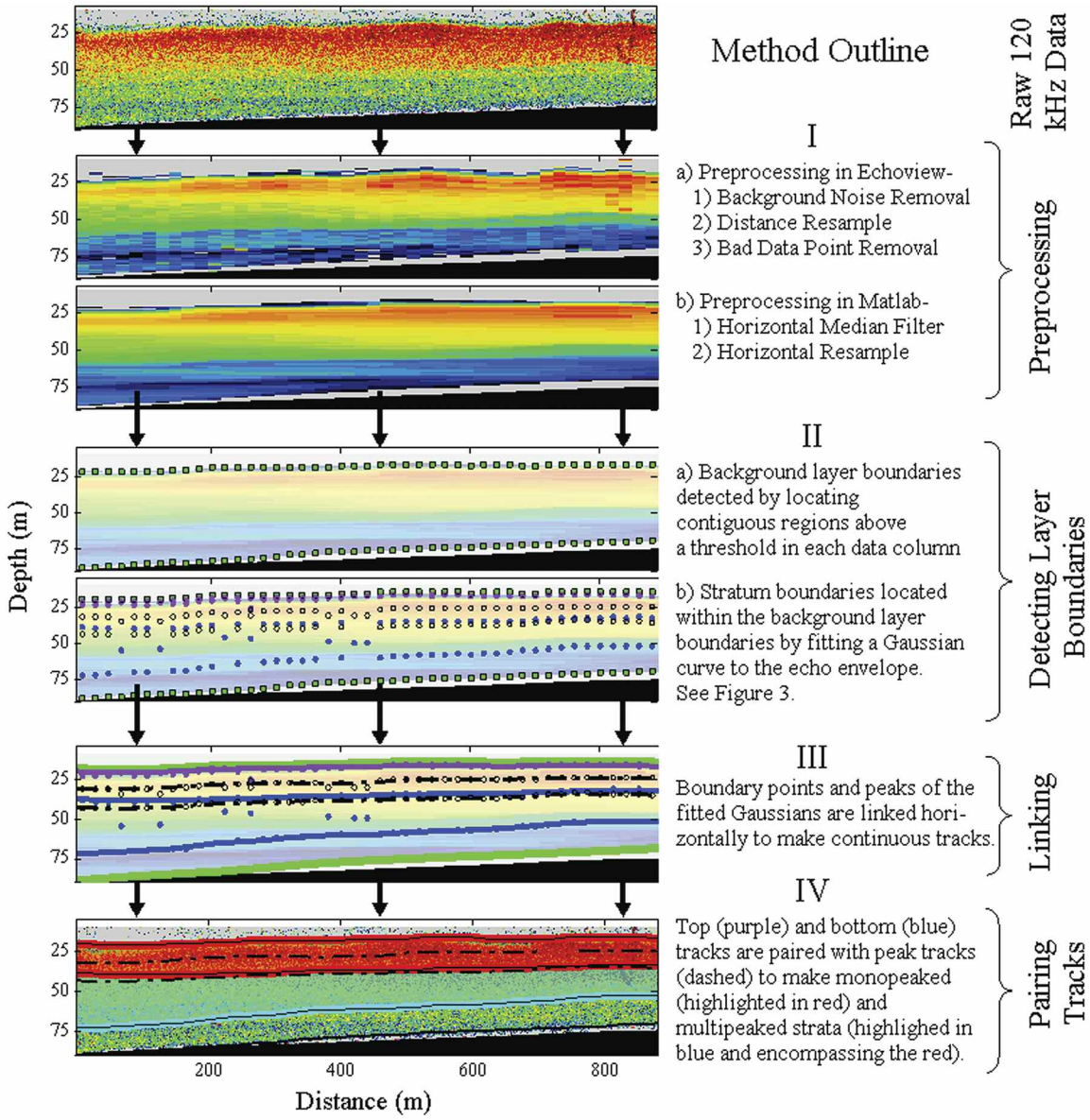


**Fig. 2.** General outline of the layer detection method in four steps. Depicted is an 850 m section of Monterey Bay data from the 10 km point of Fig. 6C. "Raw" data in panel 1 is $S_v$ data, with color scale as in all other figures. (IIa) Green squares = background layer boundaries for each column of data. (IIb) Purple squares = stratum tops, blue squares = stratum bottoms, black circles = peaks of fitted Gaussians.

parameters, listed in Table 1, which could be adjusted based on the question under investigation. The robustness of the algorithm to changes in input parameters was systematically explored using data from the GoC.

**Data collection**

Acoustic backscatter data were collected with four Simrad EK60 split-beam echosounders at 38, 70, 120, and 200 kHz. Transducers were mounted on a single pole and deployed at 1.5 m beneath the surface. Echosounder characteristics are listed in Table 2 and described by Benoit-Bird and Gilly (2012) for the GoC, by Benoit-Bird et al. (2011) for the PI, and by Benoit-Bird et al. (2009) for MB. During each experiment, the echosounders were field-calibrated using a 38.1 mm diameter tungsten carbide sphere with a target distance of 10-12 m (Foote et al. 1987).

**Preprocessing**

Standard acoustic tools were used to prepare the data for analysis. The depth of the seafloor was initially determined using Simrad EK60 software and then checked manually, and data below the seafloor were excluded from analysis. Background noise was removed via the background noise removal tool in Echoview using a maximum noise threshold of –125 dB re 1 $m^2$ $m^{-3}$ and a minimum signal-to-noise ratio of 10 dB (following De Robertis and Higginbottom 2007). At the depths

**Table 1.** Input parameters used for layer detections in Figs. 1, 2, 3, 6, and 7. Numbers below the location refer to the figure number for which these parameter values were used. The last column displays the range tested in the sampling-based sensitivity analysis. The OAT analysis used the same range except max horizontal linking distance range was 0.4-2.8 km and horizontal minimum layer length was 0.4-7 km. These values were slightly different because for the OAT analysis, the preprocessing average parameters were fixed as the distance parameters varied. "Samples," when used in the unit column, refers to a collection of sequential acoustic pings that have been averaged together horizontally across space or time. (GoC = Gulf of California, MB = Monterey Bay, PI = Pribilof Islands.)

| | | GoC | MB | | PI | | | Range tested in GoC |
|---|---|---|---|---|---|---|---|---|
| **Parameter** | **Units** | **1, 3** | **6B** | **2, 6C** | **7A** | **7B** | **7C** | **sensitivity analysis** |
| Horizontal averaging | m | 20 | 20 | 20 | 20 | 10 | 2 | 20, 25, 27.5, 30, 35 |
| Horizontal median filter | samples | 11 | 5 | 11 | 11 | 19 | 1 | 1-21 (odd) |
| Preprocessing horiz. average | samples | 7 | 4 | 1 | 7 | 7 | 2 | 1-15 (integers) |
| | (m) | (140) | (80) | (20) | (140) | (70) | (4) | |
| Threshold | dB re 1 $m^2m^{-3}$ | –78 | –78 | –78 | –78 | –78 | –78 | –83 — –70 |
| Min. layer thickness | m | 12 | 6 | 6 | 12 | 6 | 6 | 4-40 (even) |
| Max. gap within a background layer | m | 20 | 8 | 8 | 20 | 8 | 8 | 10-30 (integers) |
| Max. horiz. linking dist. | samples | 84 | 48 | 12 | 84 | 140 | 12 | 0.2-2 |
| | (km) | (1.68) | (0.96) | (0.24) | (1.68) | (1.4) | (0.02) | |
| Max. vertical linking dist. | m | 50 | 12 | 20 | 50 | 12 | 4 | 7-70 (integers) |
| Horiz. min. layer length | samples | 168 | 160 | 40 | 168 | 280 | 320 | 1-10 (km) |
| | (km) | (3.36) | (3.2) | (0.8) | (3.36) | (2.8) | (0.64) | |
| Min. vertical separation | m | 10 | 4 | 8 | 10 | 4 | 4 | 5-20 (integers) |

**Table 2.** Pulse lengths (in μs) of echosounders used in each research cruise (Benoit-Bird 2009; Benoit-Bird and Gilly 2012; Benoit-Bird et al. 2011). The nominal 3 dB beamwidth is shown for each transducer. (GoC = Gulf of California, MB = Monterey Bay, PI = Pribilof Islands).

| | Transducers | | | |
|---|---|---|---|---|
| Location | 38 kHz (12°) | 70 kHz (7°) | 120 kHz (7°) | 200 kHz (7°) |
| GoC 2011 | 512 | 512 | 512 | 512 |
| MB 2005 | 256 | 128 | 64 | 128 |
| PI 2008 | 256 | 256 | 256 | 256 |

and frequencies we examined, the effect of this step was minimal. All data were visually inspected for anomalies such as false bottom detections, noise spikes, or tracks of profiled instruments, and anomalous data were replaced with averages of the surrounding data. Like most analyses done on acoustics data, layer detection could not be completed on data that were overly noisy in which echo returns from organisms could not be distinguished from acoustic artifacts. In Fig. 1A, these excluded noisy regions are depicted as dark gray boxes, some of which extend for the entire water column for a short series of pings.

Processed volume scattering values ($S_v$ in dB re 1 $m^2$ $m^{-3}$) were averaged in the linear domain (as $s_v$ in $m^2$ $m^{-3}$) into bins of 1 m depth by a user-defined horizontal distance (as in Table 1). Horizontal distance-based bins were used to facilitate comparisons across field experiments; however, for layer detection in general, averaging by number of pings or by time interval could be used with equal facility so long as the averaging results in bins with enough independent samples of the backscattering to account for the stochastic nature of volume scattering (Simmonds and MacLennan 2005). For the remainder of the text, these averages of consecutive pings into bins are referred to as vertical columns of data, and Fig. 2 shows the results of averaging in part I(a).

Processed $S_v$ values were then exported from Echoview for further analysis in MATLAB, where the data were linearized, and two additional preprocessing steps were applied to the resulting volume backscattering coefficients ($s_v$). First, a moving horizontal median filter (Table 1) was applied to remove independent regions of high echo strength (e.g., from an individual, intense scatterer) while simultaneously smoothing the edges of continuous features to facilitate layer detection (step I(b) in Fig. 2). Second, the overall number of vertical columns was reduced by horizontal averaging to both reduce processing time and to provide additional smoothing to layer edges. Processing time was a significant consideration as averaging across seven columns, for instance, reduced run-time for the data in Fig. 1 from 6.25 h to 31 min.

**Layer detection**

After preprocessing the data, the detection of layers involved two stages: detection of potential layer edges within vertical columns of data (step II in Fig. 2) and then horizontally linking those boundaries (step III). The edge detection step used different approaches for each of two types of scattering layers: "background layers" and "internal strata." Background layers (Fig. 1B) were considered to be contiguous regions of the water column with minimum height and length

that had echo strengths above a user-defined threshold without regard for internal structure. The strong, consistent internal features found within the background layers were defined as strata (Fig. 1C). To detect the background layers, a threshold appropriate for the data was needed. Because we were interested in detecting all organisms that might aggregate in layers, we used a range of threshold values (–83 to –70 dB, see Table 1) more appropriate for small zooplankton. These thresholds were generally lower than those used in the aggregation detection algorithms for larger fish (–70 to –60 dB; Burgos and Horne 2007). After each column of $S_v$ data were smoothed with a three-point moving mean, contiguous sections of echoes with amplitude greater than the threshold were located, but sections that did not meet the user-defined minimum layer thickness criteria (see Table 1) were ignored. Features were defined as contiguous if gaps were smaller than the gap parameter.

After background layer boundaries were located in each column of $S_v$ data, the data within the boundaries were examined for potential stratum edges (step II(b) in Fig. 2). To provide a standardized, easily reportable definition of stratum boundaries, edges were identified by fitting a Gaussian curve or several Gaussian curves to regions of increased energy in the background layer (Fig. 3), and then calculating the points that

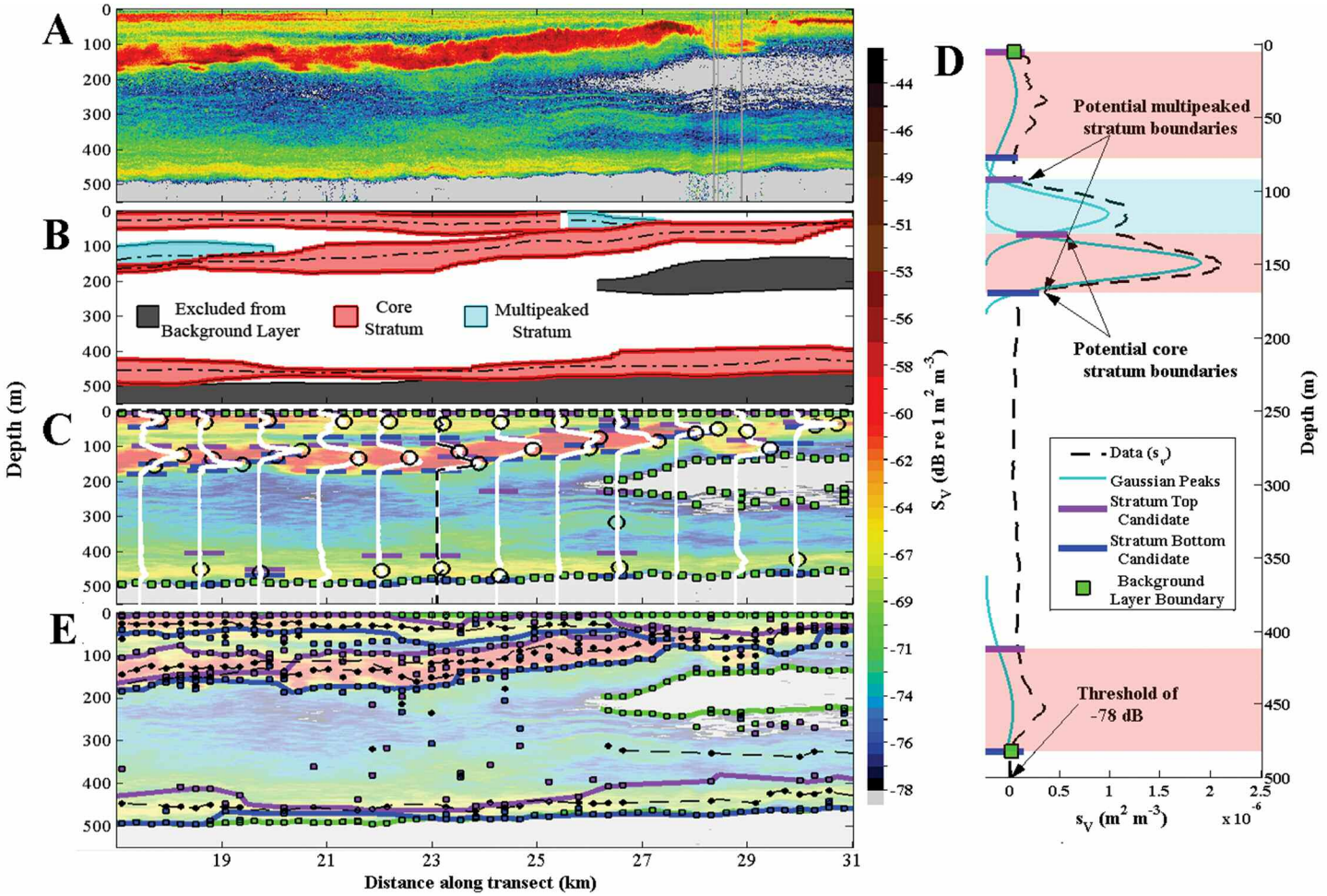


**Fig. 3.** Locating layers and strata within an echogram. (A) 14 km transect section of Fig. 1 showing upward vertical migration. (B) Scattering layers from panel A highlighted as in Fig. 1C. (C) The background echogram shows the result of applying a median filter to the $S_v$ data. The usefulness of this filter is apparent by comparing to panel A. Many isolated regions of high echo strength are absent and layer features are smoothed, leading to more consistent layer boundary detection. In each vertical column, potential background layer boundaries (green squares), stratum boundaries (purple and blue lines), and peaks of fitted Gaussians (black circles) are identified. The echo amplitudes of each data column (white lines) are plotted in the linear domain with a scale appropriate for display. For clarity, only every eighth column is graphed and every second background layer boundary candidate is displayed. The column with the dashed line is displayed in panel D. (D) A data column (in linear $s_v$ space) fitted with the Gaussian peaks whose sum best matches the original data. From these peaks, stratum boundaries are calculated as the depths that would contain 95% of the area under each curve. The displayed peaks are offset from the data for clarity. (E) Boundary candidate points are connected with a tracking algorithm. The dotted black line connects the peaks of the Gaussians. Other line colors as in panel D. The tracking algorithm must effectively track regions with a high density of points (i.e., the upper 200 m) and sparse points (i.e., the bottom 100 m), and must monitor strata as they separate and merge as at the 27 km mark. Echo strength colors are faded and every second candidate point is omitted for display clarity.

would contain 95% of the area under the curve (Fig. 3D). A peak-fitting algorithm (available at: www.mathworks.com/matlabcentral/fileexchange/23611-peak-fitter) was adapted so that up to five Gaussian curves were fitted in each analyzed section. Curves were fit by finding the combination of curves whose sum minimized the percent root mean square difference from the original data. To report the width of each curve, this algorithm output the value (in m) of the full width at half maximum (*FWHM*) of each peak. The standard deviation ($\hat{s}$) of the equation used to create the curve was calculated from the relationship between the FWHM and the standard deviation of a normal distribution:

$$\hat{s} = \frac{FWHM}{2\sqrt{2\ln(2)}} \quad (1)$$

The distance (in m) from the peak to the depths that would constrain 95% of the area of the normal curve could then be calculated by multiplying $\hat{s}$ by 1.96. To prevent over-fitting, only fitted peaks that had *FWHM* greater than half the minimum layer thickness parameter or whose peak energy value was more than five times (~7 dB) the acoustic threshold (Table 1) were kept. Five curves was chosen as the cutoff level because extra iterations of the fitting algorithm with more curves greatly increased algorithm run time without appreciably increasing fit. To increase the efficiency and facility of the Gaussian fitter, a simple peak detector algorithm (available at: www.mathworks.com/matlabcentral/fileexchange/25500-peakfinder), which identified peaks as regions that had 10 times the acoustic energy of the background layer threshold (equivalent to a 10 dB difference), was first run on the data between the background layer boundaries in each vertical column so that potential peaks could be input as starting values to the Gaussian fitter; however, the fitter was not limited to locating curves around these points.

The set of curves that best fit the data column often had overlapping 95% area boundaries. Isolated peaks and the largest peak in a set of overlapping curves were used to define and track 'core' strata (red boundaries in all figures). In cases where the boundaries of a core stratum overlapped with smaller peaks in the echo amplitude, we also tracked the boundaries of the outer edges of these overlapping peaks (Fig. 4). These strata, which contained the core strata but had expanded boundaries, we called 'multipeaked' (the expanded boundaries are blue in all figures). The structure of multipeaked strata was more complicated than that of the core strata, but their boundaries were still consistent.

Once all columns of data were analyzed for potential layer edges (Figs. 3D and 4A), the identified boundaries were linked together horizontally as in Figs. 3E and 4B, using techniques associated with particle tracking. There are many ways to approach particle tracking (e.g., Adrian 1991; Salamon et al. 2006); our approach was an adaptation of a simple tracking method (available at www.mathworks.com/matlabcentral/fileexchange/34040-simple-tracker), which operates on a frame-by-frame basis where a frame in our data were equivalent to a vertical column of potential boundary points. The horizontal

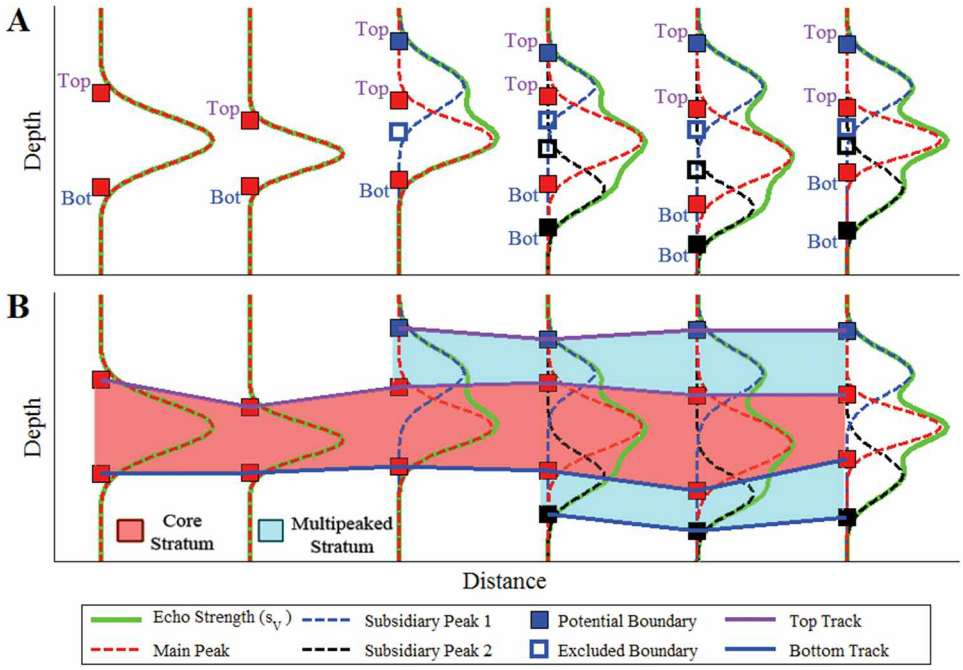


**Fig. 4.** Detecting strata. Depicted are representative echo amplitudes for six vertical columns of data. (A) 95% area boundaries of a core stratum are shown with red boxes. Overlapping subsidiary peaks are shown in columns three through six in black and blue. 95% area boundaries for the overlapping peaks are only kept as boundary points (of a potential multipeaked stratum) if they do not occur within the boundaries of the core stratum. (B) Top tracks and bottom tracks are paired to create a core stratum (red). The multipeaked stratum (in blue) that starts in column three includes the cores stratum.

distance between two successive frames and the vertical distance between two potential boundary points were dependent on the size of the bins originally chosen for averaging $S_v$ samples. This algorithm links a point in one frame to a point in the next if they are the closest pair in space and are within set linking parameters (like those in Table 1). Our algorithm extended this method by considering all of the potential boundary points in the first frame as potential tracks and then looking not only at the subsequent frame, but also at all frames within the horizontal linking distance to find the closest point. To find the closest point, the vertical and horizontal distances between two points were scaled by the corresponding max linking distance parameters (Table 1) so that the Pythagorean "distance" between two points was

$$dist = \sqrt{\frac{xdist^2}{MHLD^2} + \frac{ydist^2}{MVLD^2}} \quad (2)$$

where *xdist* is the horizontal distance between two points, *ydist* is the vertical distance, *MHLD* and *MVLD* are the max horizontal and max vertical linking distances, respectively, and *dist* is the distance that was minimized.

As the algorithm considered the potential boundary points of each frame, it kept track not only of the point it chose as closest to the point in the last frame, but also to other points that met the linking criteria. If the chosen connector point did not itself connect to a future point, the other potential connecting points were considered. The algorithm always attempted to connect the longest tracks to future points before it connected shorter tracks and as yet unconnected points. If tracks of points ended before they met the minimum layer length criteria, they were discarded. When two tracks converged so that they were within the defined minimum vertical separation distance (Table 1), in the region of overlap the longer track was prioritized. If both tracks would be longer than the minimum layer length criteria even if the region of overlap was excised, the track generated by the higher amplitude peaks was prioritized in the region of overlap.

Slightly different results were sometimes obtained if the linking algorithm started from the end of the dataset and linked points backward in time. Where the forward and backward versions were not equivalent, the two versions were merged such that the longest, most continuous tracks were kept. If two tracks converged within the minimum separation distance (Table 1), the region of the shorter track that overlapped with the longer track was excised. To define layers from the tracked boundaries (step IV in Fig. 2), the top tracks were paired with the bottom tracks and the region between them was considered part of the layer. The background tracks were paired first and then the stratum tracks were constrained to be within the background layers. If there were two consecutive stratum top tracks or stratum bottom tracks arranged vertically in the water column without the other in between, the outer track was identified as the boundary of a multipeaked stratum. For display purposes in all figures, the tracks were smoothed with a three-point moving mean filter.

**Describing layer characteristics**

Layers and strata can be quantitatively described with both geometric and acoustic measurements. For the purpose of analyzing the consistency of the algorithm, for each feature we calculated the cross-sectional area on the echogram ($m^2$), total length of the upper and lower boundaries (km), average depth (m), mean layer thickness (m), variance of the layer thickness ($m^2$), the tortuosity of the boundaries (the percent increase in boundary length compared with the shortest point between its endpoints), and for ease of comparison to previous studies, we used the nautical area scattering coefficient, an areal measure of acoustic energy ($s_A$ in $m^2$ $nmi^{-2}$) calculated from the original $S_v$ data before any filtering was applied.

We used the normality of each identified stratum as a simple proxy measure of how well the vertical distribution of scattering intensity within layers could be described by a normal curve by calculating the mean squared error (MSE) between a standardized normal curve and data that had been standardized. For each type of stratum, we defined the average departure from normality, $\Delta N$ in $m^{-2}$, as the average over all strata of the mean squared residuals from the raw $s_v$ data to the fitted Gaussians scaled to a probability density function with area 1:

$$\Delta N = \frac{1}{n}\sum_{i=1}^{n}\left(\frac{s_{Vi} - \widehat{s_{Vi}}}{\max\left(\widehat{s_V}\right) \times \hat{s} \times \sqrt{2\pi}}\right)^2 \quad (3)$$

where $\hat{s}$ is the standard deviation from Eq. 1, $\max(\widehat{s_V})$ represents the peak height of the fitted curve, and $s_{Vi}$ and $\widehat{s_{Vi}}$ are the data and the corresponding value of the fitted curve for each of *i* depth bins (Fig. 5). A single $\Delta N$ for each stratum type was calculated by averaging all $\Delta N$ for each data column in all strata of each type. Typical values were on the order of $10^{-5}$ $m^{-2}$.

Before calculating $\Delta N$, a mean filter was run over the data to minimize outlier effects and to smooth edges. To determine an appropriate window size for the mean filter, we iteratively increased the window size and calculated the correlation ($R^2$) between successive iterations for 2996 individual $\Delta N$ calculations for the monopeaked strata in Fig. 1. A window of size *n* averaged *n* points to each side of the point in question. Correlations between windows of size 1 and 2, 2 and 3, and 3 and 4 were all > 0.8, whereas correlations outside this range were much smaller, suggesting that window sizes of 1 to 4 were appropriate for this data. A window of size 1, resulting in averaging over a 3-point window, was chosen for the final analysis since greater smoothing resulted in smaller $\Delta N$ values, thus sacrificing some of the non-normality for which this parameter was designed to measure.

**Sensitivity analysis**

To test the robustness of our layer detection algorithm to changes in input parameters, two sensitivity analyses were performed using the 150 km transect section from the GoC in

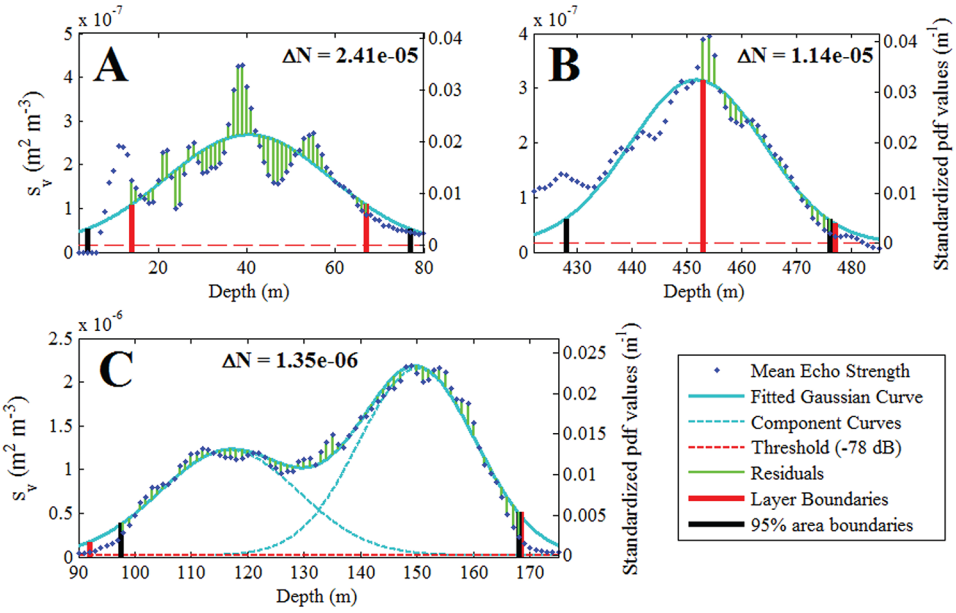


**Fig. 5.** Calculating the departure from normality (Δ*N*) for the three strata in the vertical $s_v$ data from the indicated column in Figs. 3C and 3D. Red lines in the figure are the boundaries of the stratum, which depend not only on this column, but also on data from surrounding columns. This dependence explains why they do not match the 95% Gaussian area boundaries, which are determined from the fitted curves and represent the boundaries containing 95% of the area of the curve. If the 95% boundaries are within the layer boundaries, the innermost boundaries are used as endpoints for calculating Δ*N* to minimize the effect of outliers well away from the main energy of the stratum. $s_v$ values are shown on the left axis, whereas standardized values are displayed on the right axes. (A) A shallow core stratum that demonstrates a moderate Gaussian fit. (B) A deep core stratum that has a good fit. Note that removing the three shallowest data points gives Δ*N* = 4.16e-06, so a few strongly non-normal data points can have a large contribution to Δ*N*. Also note that because the peak in the Gaussian curve at 452 m is not within the layer boundaries, this Δ*N* would not be included in the average calculated for all core strata and would be recorded as having a non-Gaussian fit. (C) In multipeaked strata, a number of curves corresponding to the number of detected peaks were fit to the data. Residuals were calculated from the standardized sum of those curves. Standardization in this case still resulted in an area of one under the summed curves. Note: in the actual layer analysis of this section of data, only the boundaries of the largest peak in this section were tracked because only the core stratum was consistent in surrounding data columns. Two curves were included here, however, to demonstrate the calculation of Δ*N* for the overlapping curves of multipeaked strata.

Fig. 1 as an example region. Layers and strata were characterized with the geometric and acoustic measurements described above as well as with the total number of tracks detected by the algorithm. The changes in these measurements were monitored as input parameters were varied. A one-at-a-time (OAT) sensitivity analysis was performed to unambiguously determine the effects of single inputs on the descriptive parameters. Starting at the baseline values for the GoC used to create Fig. 1, input parameters were varied through a range of values. The limits of this range were selected so as to include broadly applicable values that might be useful for investigation of layers that range in thickness from meters to tens of meters, but also to keep the number of runs of the algorithm to a reasonable size. For the OAT analysis, a total of 227 runs were performed on the GoC data in Fig. 1 and the effect of the change in input parameter on each output parameter was recorded.

To examine patterns in layer detections resulting from parameter changes, a sampling-based sensitivity analysis was employed using a size-200 Latin hypercube sample (McKay et al. 1979) drawn from the same data ranges as the OAT analysis (except as described in Table 1). To quantify the effect of each input parameter on each output parameter, we used several metrics described in Helton and Davis (2000) including partial correlation coefficients (*PCC*), the standardized regression coefficients (*SRC*) of a multiple linear regression model, changes in $R^2$ excluding each input value ($R^2$-*del*), and the *SRC* from stepwise models. To look for nonlinear trends, we calculated Spearman's ρ for each input/output pair and also performed all of the above tests again after ranking the data. Finally, to look for non-random patterns that may not have been monotonic, a $\chi^2$-test for nonrandom patterns was performed on plots of each input/output pair.

## Assessment

To examine the effectiveness of the algorithm, we first visually examined the automatically detected layers in echograms from three diverse habitats. The layers and strata detected automatically in Figs. 1, 3, 6, and 7 closely matched features that an observer would visually identify as scattering layers. The top depth, bottom depth, and peak energy depth of multiple layers were effectively tracked, even as their structures and properties varied across space and time. The regions in these figures were

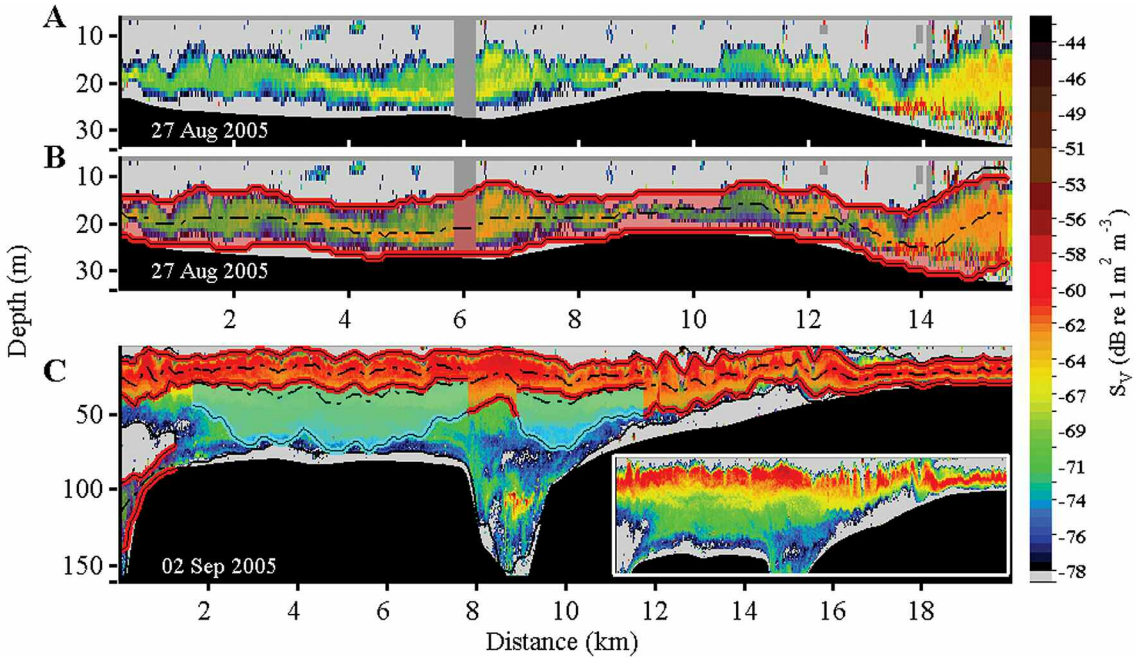


**Fig. 6.** Two sections of transects in Monterey Bay, California collected at 120 kHz. Monterey Bay is a productive, temperate coastal embayment with aggregations of anchovies (*Engraulis mordax*), sardines (*Sardinops sagax*), and small crustaceans including copepods (Benoit-Bird 2009; Kaltenberg and Benoit-Bird 2009). (A) A thin (<10 m) layer of microorganisms with high backscatter at 120 kHz that does not appear in lower frequency echograms taken simultaneously. (B) The superposition of the detected layer over the echogram in panel A, it showcases the ability of the algorithm to detect thin layers close to the ocean floor. The detected stratum takes up almost the entire background layer, denoted with black lines. (C) A 120 kHz echogram showing how the algorithm can detect a thin stratum at the top of a larger background layer even as it approaches the ocean bottom. Also depicted is a benefit of this detection method over threshold-based methods since the stratum at the bottom left corner is also detected despite having a much lower average $S_v$. The inset is the same region without the layers superimposed.

chosen to test the algorithm's flexibility in working on data with diverse scattering layer structure, dynamics, and constituents. To highlight this flexibility, Fig. 7 shows data for which adjusting the input parameters of the algorithm could define scattering layers according to differing research objectives: it could be used to spatially connect discrete, but closely spaced, asymmetrical aggregations of pollock (Figs. 7A & 7B), or to separate out only the contiguous, symmetrical features more characteristic of scattering layers (Fig. 7C).

The problem of standardizing layer boundaries was addressed by applying a normal curve to vertical columns of data. Because of its generality, applying a Gaussian distribution function facilitated comparisons across the range of environments that we examined. By using the sum of several Gaussian curves, even the boundaries of layers that were not symmetrical could be located; if the depths of those boundaries were stable over time, a multipeaked layer was identified (Fig. 4). Using Gaussian curves to describe scattering layers also ensures that the parameters used are easily reported and conceptualized, providing standardized tools for classifying and identifying scattering layers. To determine how well the simple approach of describing internal strata with Gaussian distributions characterized real features, we compared each vertical column of each stratum in Fig. 1 to the distribution of a normal curve using a Pearson's $\chi^2$ test, calculating a $p$ value for the null hypothesis that the "sample" was drawn from a population with a normal distribution. With no data smoothing and no outliers removed, 91% of the 3044 vertical columns had $p > 0.8$, suggesting that the majority of internal strata were well described with easily interpreted Gaussian curves. Fitting a normal curve even to skewed data should appropriately identify the peak and give an approximation of the boundaries of the peak energy, excluding only a small amount of the total energy within an identified layer. Although more complex probability density functions might increase the overall fit of the curves to the observed distribution of echo amplitudes in some circumstances, our fundamental understanding of how organisms are arranging themselves within layers may be obscured by the challenges of interpreting these more complex models.

To test the robustness of the algorithm to changes in input parameters, we conducted two sensitivity analyses on data from the GoC. These results demonstrated the robustness of the algorithm and provided details for establishing guidelines for selecting and reporting input parameters when applying the algorithm. Thirty-one output parameters were tested for their sensitivity to changes in ten input parameters. The results are summarized in Fig. 8 and detailed in Web Appen-

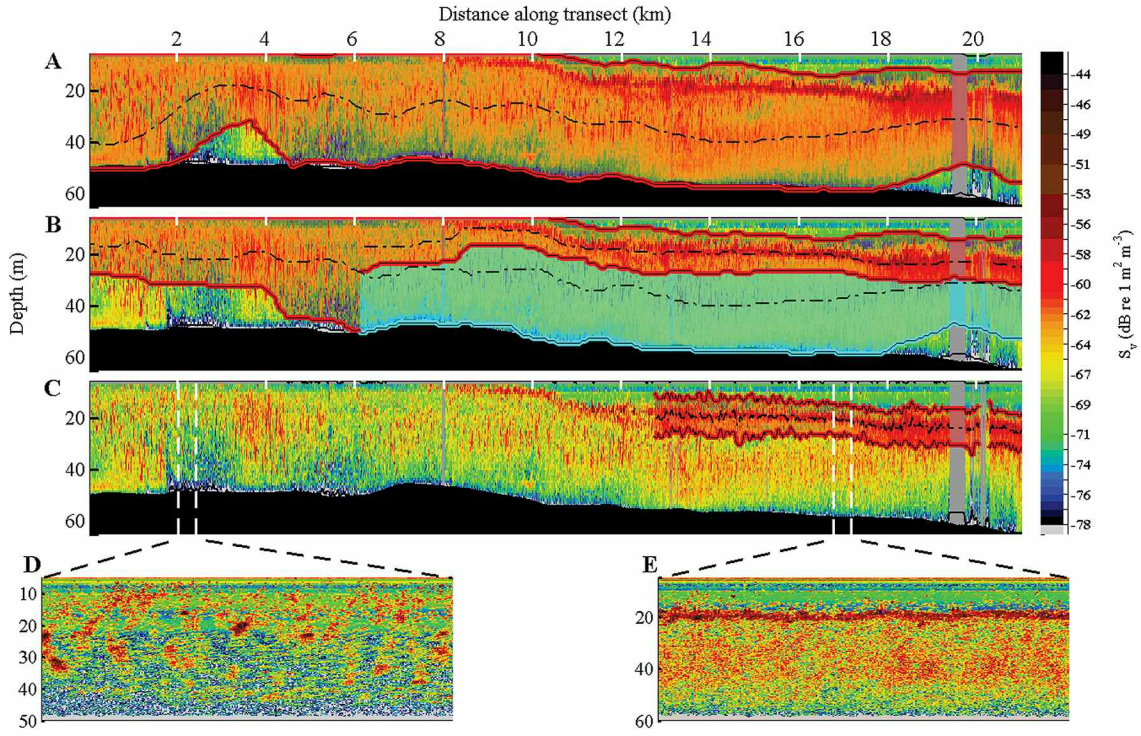


**Fig. 7.** A 21 km transect of 38 kHz data collected near the Pribilof Islands in the Bering Sea. Primary biologic constituents are young-of-the-year walleye pollock (Benoit-Bird et al. 2013). Settings for the layer detection algorithm can be adjusted to track different types of biology with different aggregating characteristics (values in Table 1). In all figures, the background layer encompasses almost the entire water column. In (A), settings are the same as in Figs. 1 and 3 for the GoC. They emphasize thick, long strata and count neighboring patches as part of a layer. (B) Settings allow for detection of thinner strata, but still link patches. (C) Settings allow for detection of thin strata and identify only those that match the definition of a layer as a region that cannot be individually resolved (as per Tont 1976). (D) The leopard spotting pattern in a raw echogram typical of young-of-the-year pollock. (E) A section of transect with more typical layer characteristics.

dix 1. Most of the variables were relatively insensitive to changes in input (white boxes), changed predictably in response to changes in input parameters (green boxes), or had reduced output variation when the input range was restricted by 25% or 50% (removable and moderately removable variation-striped boxes). For example, increasing the threshold for including data should naturally result in a smaller area incorporated within the detected layer. Red boxes highlight where particular care must be taken in selecting parameters and interpreting the results because effects were substantial, unpredictable, and occurred throughout the tested range of the input parameter.

Of the 310 tested input/output pairs, 44 (14%) fell into one of the unpredictable categories. Of these 44 pairs, 16 were associated with the number of tracks output parameter, 13 with the variance of the layer thickness, and 11 with tortuosity. Area, length (in all but one case), depth, thickness, $s_A$, and 17 out of 20 $\Delta N$ calculations were all not substantially affected by changes in input or were affected in predictable ways. The acoustic energy measurement $s_A$, calculated from unfiltered $S_v$ data within the calculated layers, was largely unaffected by changes in input parameters; 28 of 30 input/output pairs did not vary substantially (<20% output variation) and restricting the range of the max vertical linking distance to 84% (core strata) and 94% (multipeaked strata) reduced the output variation below the 20% threshold for the two remaining pairs. Sixty percent of the $s_A$ pairs met even a reduced (<10%) criteria for substantial variation.

A key advantage of this algorithm is that the major characteristics of the background layers and strata were not unpredictably affected by the choice of threshold or other input parameters. With the exception of 1 out of 60 length parameters and 3 out of 20 $\Delta N$ parameters, the only unpredictable and significant responses of outputs to changes in input related to features (tortuosity, variance of layer thickness, and number of tracks) that are not the focus of most research interests, but were included in our analysis as additional metrics of layer characteristics and algorithm stability. Our algorithm used horizontal averaging to smooth edges and find more consistent boundaries, and this approach came at the cost of less precise tortuosity and variance of layer thickness measurements.

The output parameter most unpredictably affected by changes in input parameter was the number of tracks

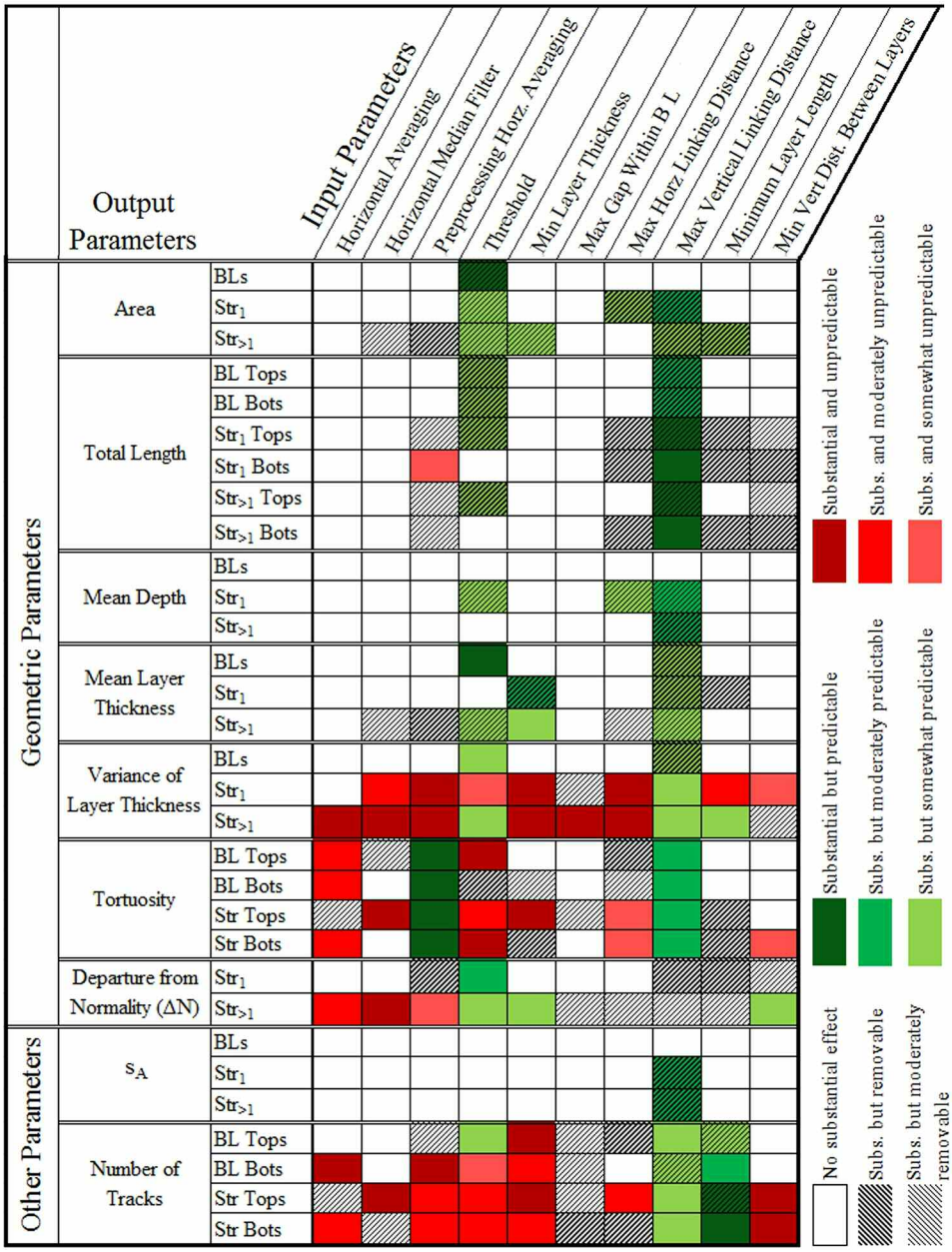


**Fig. 8.** Results of two sensitivity analyses performed on the data from the Gulf of California displayed in Fig. 1 using input parameter ranges listed in Table 1. The effect on each output parameter of varying each input parameter is indicated. Output parameters are in the rows, input parameters in the columns. White, striped, and green categories imply the algorithm was robust for these input/output pairs. Red implies that these parameter pairs may give inconsistent results from trial to trial. BL = Background Layers. $Str_1$ = Core Strata. $Str_{>1}$ = Multipeaked Strata. Full descriptions and the raw data used to create these categories are available in Web Appendix 1.

parameter. The number of tracks identified was a reflection of how changing the input parameters affected how potential top or bottom boundary points were linked. However, the stability of other parameters despite an unpredictable overall number of tracks suggests that the number of tracks did not largely affect the final identification of background layers or strata. It is likely that small gaps in the boundaries increased the number of tracks, but did not greatly affect the characteristics of the layers and strata. This is an important attribute since small gaps that may exist in a two-dimensional echogram are likely only small holes in a larger three-dimensional pancake-shaped layer (Reid et al. 2000) or are the results of gaps in data from noise removal or surface bubbles.

Despite the unpredictable effects on tortuosity, number of tracks, and variance of layer thickness, our algorithm was

robust. It is significant, for instance, that total acoustic energy in the layers was largely unaffected by changes in input parameter, including threshold choice. This is perhaps not surprising as the range of acoustic thresholds tested did not approach the levels necessary to exclude regions of concentrated gas-bearing organisms that can be the main components of scattering layers. This choice was made so that the actual characterization of scattering layers would rely on the organization of echoes within the layer, not on the acoustic threshold. This result implies that the algorithm could be used to automatically and consistently measure biomass that exists exclusively within scattering layers over large regions. Large-scale biomass surveys could benefit from the classification of echo energy into scattering layer bins instead of depth bins as is commonly done (e.g., Kloser et al. 2009). The robustness of our algorithm also suggests that it would be effective in regions where the organisms of interest change, and it enables comparisons between sites.

## Discussion

The mid-trophic level residents of acoustic scattering layers play key roles in oceanic environments. Despite being some of the most abundant organisms in the oceans, they are also among the least studied (Catul et al. 2011). Because of the challenges in monitoring these ubiquitous organisms at large scales, a current research priority is the creation of new tools for that purpose (Lehodey et al. 2010). To meet this need, our goal was to develop an automatic detection algorithm that could consistently define and describe scattering layers while being robust to changes in the specifics of site, species, and layer behavior. The algorithm we have presented has the benefit of being applicable not just to the analysis of new data, but also to the processing of datasets that have already been collected, allowing researchers to gain new insights from old data.

The method we described improved on older methods since it was designed to address scattering layers specifically, in a variety of environments. The layer detection algorithm is automatic and objective, addressing the potential bias of visual examination, and it works by detecting both top and bottom boundaries and is not limited in horizontal extent. Although the Gaussian peak detection takes advantage of an energy differential to locate regions of high acoustic energy as an algorithmic starting point, the algorithm presented here eliminates the reliance on a background noise differential in *characterizing* peaks, which most previously described algorithms use. The difficulty of choosing an appropriate acoustic threshold is addressed in that the detection of internal strata, usually the type of layer of primary biological interest, relies on the depth distribution of the echoes within the layer, not directly on the acoustic threshold chosen. The primary effect of acoustic threshold choice in our algorithm was on the size of the background layers which then constrained the size of the strata; $s_A$, in contrast to other methods, was not substantially affected. The linking algorithm used is an approach to particle tracking that appropriately deals with commonly encountered anomalies such as scattering layers that split, merge, have gaps, and gradually get more diffuse over time.

To compare the vertical profile of acoustic scattering in a layer to a normal distribution, we measured a parameter, $\Delta N$, that allows for comparisons of the normality of data with amplitudes that could differ by orders of magnitude. As has been done for fish schools (Scalabrin et al. 1996), characterization of the internal organization within scattering layers may ultimately be useful for the separation of the constituent organisms by types or sizes. In addition to providing a measure of the choice of fitting function (in this case Gaussian), $\Delta N$ was a useful proxy metric of layer shape, giving a simple numerical representation of the distribution of scattering in the layer. A quantitative measure of the non-normality like $\Delta N$ makes comparing the normality of layers in different locations or environments much more straightforward than goodness-of-fit tests that rely on the calculation of a $p$ value, and a similar metric could be employed with equal facility if a different probability density function (PDF) is used in its place.

The algorithm we have described consistently identified the boundaries of acoustic scattering layers, was robust to different types of acoustic scatterers and input parameters in disparate ecosystems, could be used to describe a variety of layer characteristics, and could monitor layers over extensive horizontal distances. The use of automated acoustic scattering layer detection tools, such as the one outlined here, will allow for more complete and consistent characterizations of the acoustic and geometric properties of scattering layers than has been attempted previously, an important step for describing their role in oceanic ecosystems. Widespread use of a consistently applicable layer detection method and descriptive characters provides a way to compare characteristics of scattering layers across ecosystems and between studies. There is much about how the organisms in scattering layers interact with each other and their environment that remains obscure, but adoption and application of the method that we have described would help shed light on these interactions.

## Comments and recommendations

Like most acoustic analyses, it is important to preprocess and calibrate raw data thoroughly before attempting to apply our algorithm. Scattering that appears below the depth of the seafloor and acoustic anomalies that do not represent aggregations of organisms should be removed. Although the algorithm is adept at separating layers from other types of biological acoustic scattering, excessive noise can blur boundaries and layer detection may give inconsistent results if noisy regions cannot be removed. However, as shown by the gray regions in Fig. 1, if noisy regions can be isolated and replaced with averages of the surrounding data, the algorithm presented here can successfully monitor layers through intermittent problem regions.

It is useful for the application of this algorithm to be aware that changing the threshold and maximum vertical linking distance parameters can have a predictable effect on output parameters. Both of these parameters affect how much data to include in a scattering layer, and care should be taken that results of the analysis of different regions should only be compared if they use similar thresholds and maximum vertical linking distances. It is significant, however, that most of these input/output pairs are not only predictable, but also removable (Fig. 8), implying that the results are relatively insensitive to the specific parameters used and facilitating comparisons across studies. Additionally, for some research questions, the ability to affect how the algorithm defines layers is an important feature. For instance, in the region of the PI shown in Fig. 7, variations in the maximum vertical linking distance parameter contributed to the very different stratum formations identified, and gave the algorithm flexibility to attain different research objectives. In applying this method to the task of describing scattering layers, we recommend carefully reporting the input parameters used for analysis, specifically highlighting the threshold and vertical linking distance used.

Although the layer detection method we have described was designed and tested with single-frequency acoustic data in mind, the underlying principles should be applicable to a range of echograms used for backscatter classification, including broadband echograms and those that combine multiple frequencies mathematically. Readers interested in applying the method we have described may obtain further, practical details from the MATLAB code available online (Cade and Benoit-Bird 2014).

## References


Adrian, R. J. 1991. Particle-imaging techniques for experimental fluid mechanics. Annu. Rev. Fluid Mech. 23:261-304 [doi:10.1146/annurev.fl.23.010191.001401].

Baliño, B., and D. L. Aksnes. 1993. Winter distribution and migration of the sound scattering layers, zooplankton and micronekton in Masfjorden, western Norway. Mar. Ecol. Progr. Ser. 102:35-35 [doi:10.3354/meps102035].

Barange, M. 1994. Acoustic identification, classification and structure of biological patchiness on the edge of the Agulhas Bank and its relation to frontal features. S. Afr. J. Mar. Sci. 14:333-347 [doi:10.2989/025776194784286969].

Benoit-Bird, K. J. 2009. Dynamic 3-dimensional structure of thin zooplankton layers is impacted by foraging fish. Mar. Ecol. Progr. Ser. 396:61-76 [doi:10.3354/meps08316].

———, and W. W. L. Au. 2003. Echo strength and density structure of Hawaiian mesopelagic boundary community patches. J. Acoust. Soc. Am. 114:1888 [doi:10.1121/1.1612484].

———, and W. W. L Au. 2004. Diel migration dynamics of an island-associated sound-scattering layer. Deep Sea Res. I 51:707-719 [doi:10.1016/j.dsr.2004.01.004].

———, T. J. Cowles, and C. E. Wingard. 2009. Edge gradients provide evidence of ecological interactions in planktonic thin layers. Limnol. Oceanogr. 54:1382-1392 [doi:10.4319/lo.2009.54.4.1382].

———, M. A. Moline, C. M. Waluk, and I. C. Robbins. 2010. Integrated measurements of acoustical and optical thin layers I: Vertical scales of association. Cont. Shelf Res. 30:17-28 [doi:10.1016/j.csr.2009.08.001].

———, K. Kuletz, S. Heppell, and B. Hoover. 2011. Active acoustic examination of the diving behavior of murres foraging on patchy prey. Marine Ecology Progress Series 443:217-235 [doi:10.3354/meps09408].

———, and W. F. Gilly. 2012. Coordinated nocturnal behavior of foraging jumbo squid *Dosidicus gigas*. Mar. Ecol. Progr. Ser. 455:211-228 [doi:10.3354/meps09664].

———, and M. A. McManus. 2012. Bottom-up regulation of a pelagic community through spatial aggregations. Biol. Lett. 8:813-816 [doi:10.1098/rsbl.2012.0232].

———, N. E. McIntosh, and S. A. Heppell. 2013. Nested scales of spatial heterogeneity in juvenile walleye pollock *Theragra chalcogramma* in the southeastern Bering Sea. Mar. Ecol. Progr. Ser. 484:219-238 [doi:10.3354/meps10319].

Bertrand, A., M. Ballón, and A. Chaigneau. 2010. Acoustic observation of living organisms reveals the upper limit of the oxygen minimum zone. PLOS One 5:e10330 [doi:10.1371/journal.pone.0010330].

Burd, B. J., R. E. Thomson, and G. S. Jamieson. 1992. Composition of a deep scattering layer overlying a mid-ocean ridge hydrothermal plume. Mar. Biol. 113:517-526 [doi:10.1007/BF00349179].

Burgos, J. M., and J. K. Horne. 2007. Sensitivity analysis and parameter selection for detecting aggregations in acoustic data. ICES J. Mar. Sci. 64:160-168.

Cade, D. E., and K. J. Benoit-Bird. 2014. An automatic and quantitative approach to the detection and tracking of acoustic scattering layers (supplemental code). Software. Oregon State University Libraries [doi:10.7267/N96Q1V56].

Catul, V., M. Gauns, and P. K. Karuppasamy. 2011. A review on mesopelagic fishes belonging to family Myctophidae. Rev. Fish Biol. Fisher. 21:339-354 [doi:10.1007/s11160-010-9176-4].

Chapman, R., and J. Marshall. 1966. Reverberation from deep scattering layers in the western North Atlantic. J. Acoust. Soc. Am. 40:405-411 [doi:10.1121/1.1910087].

Cheriton, O. M., M. A. McManus, D. Holliday, C. F. Greenlaw, P. L. Donaghay, and T. J. Cowles. 2007. Effects of mesoscale physical processes on thin zooplankton layers at four sites along the west coast of the US. Estuar. Coasts 30:575-590.

De Robertis, A., and I. Higginbottom. 2007. A post-processing technique to estimate the signal-to-noise ratio and remove echosounder background noise. ICES J. Mar. Sci. 64:1282-1291.

Duvall, G., and R. Christensen. 1946. Stratification of sound scatterers in the ocean. J. Acoust. Soc. Am. 18:254-254 [doi:10.1121/1.1902470].

Foote, K. G., H. Knudsen, G. Vestnes, D. MacLennan, and E. Simmonds. 1987. Calibration of acoustic instruments for fish density estimation: a practical guide. ICES Cooperative Research Report 144:1-69.

Hays, G. C. 2003. A review of the adaptive significance and ecosystem consequences of zooplankton diel vertical migrations. Hydrobiologica 503:163-170 [doi:10.1023/B:HYDR.0000008476.23617.b0].

Helton, J. C., and F. J. Davis. 2000. Sampling-based methods, p. 101-154. *In* A. Saltelli, K. Chan, and E. M. Scott [eds.], Sensitivity analysis. John Wiley & Sons.

Jech, J. M., and W. L. Michaels. 2006. A multifrequency method to classify and evaluate fisheries acoustics data. Can. J. Fish. Aquat. Sci. 63:2225-2235 [doi:10.1139/f06-126].

Kaltenberg, A. M., and K. J. Benoit-Bird. 2009. Diel behavior of sardine and anchovy schools in the California Current System. Mar. Ecol. Progr. Ser. 394:247-262 [doi:10.3354/meps08252].

Kloser, R. J., T. E. Ryan, J. W. Young, and M. E. Lewis. 2009. Acoustic observations of micronekton fish on the scale of an ocean basin: potential and challenges. ICES J. Mar. Sci. 66:998-1006 [doi:10.1093/icesjms/fsp077].

Kumar, P. V. H., T. P. Kumar, T. Sunil, and M. Gopakumar. 2005. Observations on the relationship between scattering layer and mixed layer. Curr. Sci. 88:1799.

Lehodey, P., R. Murtugudde, and I. Senina. 2010. Bridging the gap from ocean models to population dynamics of large marine predators: a model of mid-trophic functional groups. Progr. Oceanogr. 84:69-84 [doi:10.1016/j.pocean.2009.09.008].

Markaida, U., W. F. Gilly, C. A. Salinas-Zavala, R. Rosas-Luis, and J. Booth. 2008. Food and feeding of jumbo squid *Dosidicus gigas* in the Central Gulf of California during 2005-2007. California Cooperative Oceanic Fisheries Investigations Report 49:90-103.

McKay, M. D., R. J. Beckman, and W. J. Conover. 1979. Comparison of three methods for selecting values of input variables in the analysis of output from a computer code. Technometrics 21:239-245.

Nero, R., and J. Magnuson. 1992. Effects of changing spatial scale on acoustic observations of patchiness in the Gulf Stream. Landscape Ecol. 6:279-291 [doi:10.1007/BF00129706].

O'Brien, D. P. 1987. Direct observations of the behavior of *Euphausia superba* and *Euphausia crystallorophias* (Crustacea: Euphausiacea) under pack ice during the Antarctic spring of 1985. J. Crust. Biol. 7:437-448 [doi:10.2307/1548293].

Opdal, A., O. Godø, O. Bergstad, and Ø. Fiksen. 2008. Distribution, identity, and possible processes sustaining meso- and bathypelagic scattering layers on the northern Mid-Atlantic Ridge. Deep Sea Res. II 55:45-58 [doi:10.1016/j.dsr2.2007.09.002].

Reid, D., and others. 2000. Standard protocols for the analysis of school based data from echo sounder surveys. Fish. Res. 47:125-136 [doi:10.1016/S0165-7836(00)00164-8].

Robinson, C. J., and J. Gómez-Gutiérrez. 1998. Daily vertical migration of dense deep scattering layers related to the shelf-break area along the northwest coast of Baja California, Mexico. J. Plank. Res. 20:1679-1697 [doi:10.1093/plankt/20.9.1679].

Salamon, P., D. Fernàndez-Garcia, and J. J. Gómez-Hernández. 2006. A review and numerical assessment of the random walk particle tracking method. J. Contam. Hydrol. 87:277-305 [doi:10.1016/j.jconhyd.2006.05.005].

Sameoto, D. 1976. Distribution of sound scattering layers caused by euphausiids and their relationship to chlorophyll a concentrations in the Gulf of St. Lawrence Estuary. J. Fish. Board Can. 33:681-687 [doi:10.1139/f76-084].

Scalabrin, C., N. Diner, A. Weill, A. Hillion, and M.-C. Mouchot. 1996. Narrowband acoustic identification of monospecific fish shoals. ICES J. Mar. Sci. 53:181-188 [doi:10.1006/jmsc.1996.0020].

Simard, Y., and D. L. Mackas. 1989. Mesoscale aggregations of euphausiid sound scattering layers on the continental shelf of Vancouver Island. Can. J. Fish. Aquat. Sci. 46:1238-1249 [doi:10.1139/f89-160].

Simmonds, J., and D. N. MacLennan. 2005. Fisheries acoustics: theory and practice, 2nd ed. Blackwell Science [doi:10.1002/9780470995303].

Steinberg, D. K., C. A. Carlson, N. R. Bates, S. A. Goldthwait, L. P. Madin, and A. F. Michaels. 2000. Zooplankton vertical migration and the active transport of dissolved organic and inorganic carbon in the Sargasso Sea. Deep Sea Res. I 47:137-158 [doi:10.1016/S0967-0637(99)00052-7].

Thomson, R. E., B. J. Burd, A. G. Dolling, R. Lee Gordon, and G. S. Jamieson. 1992. The deep scattering layer associated with the Endeavour Ridge hydrothermal plume. Deep Sea Res. A 39:55-73 [doi:10.1016/0198-0149(92)90020-T].

Tont, S. A. 1976. Deep scattering layers: patterns in the Pacific. California Cooperative Oceanic Fisheries Investigations Report 18:112-117.

Weber, T. C., H. Peña, and J. M. Jech. 2009. Consecutive acoustic observations of an Atlantic herring school in the Northwest Atlantic. ICES J. Mar. Sci. 66:1270-1277 [doi:10.1093/icesjms/fsp090].

Weill, A., C. Scalabrin, and N. l. Diner. 1993. MOVIES-B: an acoustic detection description software. Application to shoal species' classification. Aquat. Living Resourc. 6:255-267 [doi:10.1051/alr:1993026].

*Submitted 18 April 2014*
*Revised 30 September 2014*
*Accepted 13 October 2014*